

Soft Matter

Accepted Manuscript



This is an *Accepted Manuscript*, which has been through the Royal Society of Chemistry peer review process and has been accepted for publication.

Accepted Manuscripts are published online shortly after acceptance, before technical editing, formatting and proof reading. Using this free service, authors can make their results available to the community, in citable form, before we publish the edited article. We will replace this *Accepted Manuscript* with the edited and formatted *Advance Article* as soon as it is available.

You can find more information about *Accepted Manuscripts* in the [Information for Authors](#).

Please note that technical editing may introduce minor changes to the text and/or graphics, which may alter content. The journal's standard [Terms & Conditions](#) and the [Ethical guidelines](#) still apply. In no event shall the Royal Society of Chemistry be held responsible for any errors or omissions in this *Accepted Manuscript* or any consequences arising from the use of any information it contains.

Quasi-2d fluids of dipolar superballs in external field

Per Linse

*Physical Chemistry, Department of Chemistry, Lund University, Box 124, SE-221 00 Lund,
Sweden*

Abstract

Structure of quasi-2d solutions of dipolar superballs in the fluid state has been determined by Metropolis Monte Carlo simulations without and with the presence of an external field. Superballs are 3d objects characterized by one shape parameter. Here, superballs resembling cubes, but possessing rounded edges, have been used. Examination has been made for several magnitudes of the dipole moment at three different dipole directions. In the limit of a cube, the directions become (i) center of mass – center of a face (001) direction, (ii) center of mass – center of an edge (011) direction, and (iii) center of mass – corner (111) direction. At a small dipole moment, the superballs are translationally and orientationally disordered, and the dipoles become partially orientationally ordered in the presence of the field parallel to the plane of the superballs. At a large dipole moment, chains of superballs are formed, and the chains become parallel in the presence of the field. The chains remain separated for the dipole in the 001-direction and form bundles for the 011- and 111-directions. The different structures obtained for the different dipole directions are interpreted in terms of how compatible the dipole-dipole interaction is with the cube-cube interaction at short separation for the different directions of the dipole moment. Hence, the structural richness appears from an interplay of the different symmetries of a cube and of the field of a dipole.

1 Introduction

Magnetic fluids, also referred to as ferrofluids, are dispersions of magnetic particles on sub-micrometer scale in non-magnetic solvents and have been subjected to many experimental and theoretical studies, see, e.g., [1], [2], [3], [4], [5]. Ferrofluids have found applications in fields such as diagnosis of diseases and their treatments, friction regulation, and bearings by forming mechanical seals preventing leakage.

Traditionally, most magnetic fluids of well-characterized particles have been composed of spherical particles with a dipole moment positioned at the center. Similarly, most theoretical and model studies have been devoted to such systems. For example, Weis [6] has simulated low-density quasi-2d system of dipolar hard spheres in a tilted external field. In particular, a threshold value of the tilt angle for a transition from a disordered state to a state of chains was observed. For larger tilt angles, the chains grew into bundles. Furthermore, Schmidle [7] et al. determined the phase behavior of a two-dimensional liquid of spheres interacting with a discontinuous potential representing that of a non-ideal dipole formed by two opposite charges using a discontinuous molecular dynamic technique. At low density and high temperature, a disordered homogeneous fluid was found; at high density and low temperature, a percolated fluid was obtained; and in between a string fluid was reported.

More recently, the activities in this field have developed in two different directions: (i) spherical particles with off-centered (shifted) location of the dipole and (ii) *non*-spherical particles with a central dipole. Novel structures are expected, in the first case from the non-superimposing centers of the sphere and of the dipole, and in the latter case from the more complex relation between the symmetry of the *non*-spherical particle and that of the dipole field as compared to the relation between the symmetry of a spherical particle and that of the dipole field.

As to shifted dipoles, Kantorovich et al. [8] have theoretically investigated the ground state for a system of a few dipolar particles with the dipole moment pointing in the radial direction of the spherical particles. Piastra and Virga [9] examined spheres located in a plane and possessing point dipoles, and they also constructed a mean-field theory for a homogeneous ferrofluid monolayer. In particular, the theory predicts a transition from an isotropic, non-polar phase to an ordered, polar phase at increasing dipolar coupling. Their theory was subsequently extended by Gartland and Virga. [10] Furthermore, Klinkigt et al. [11] investigated the cluster formation of spherical particles, again with shifted dipole moment, in quasi two-dimensional and three-dimensional systems. In consistency with Piastra

and Vigra [9], the cluster size was found to increase with increased dipolar coupling. In another simulation study, Abrikosov et al. [12] examined spheres with shifted dipoles with their dipole moments directed in different directions in a quasi two-dimensional setup in absence and presence of external fields in different directions. In particular, their results displayed several strong similarities with experiments by Sacanna et al. [13]

As to non-dipolar superballs, it appears that the theoretical interests preceded their experimental realization. Batten et al. [14] performed molecular simulations and determined the equation of state for the low-density fluid state and high-density ordered states for the full interval from cubes to spheres. In addition, the structure of the phases was characterized by radial distribution functions and orientational correlation functions. Similar examination of the phase diagram also including octahedral-shaped particles were performed by Ni et al. [15] In a subsequent study, Gantapara et al. [16] examined the phase diagram of truncated hard cubes and found a rich behaviour of different structures and phases. Finally, by molecular dynamic simulation, Knoroski and Travesset [17] examined the formation of controlled structures formed cubes with attached linkers. A protocol for formation of hollow silica cubes were presented by Rossi et al. [18] In their work, they also demonstrated the formation of cubic crystals under attractive interactions by the addition of depletant. Further studies of the crystalline structure of hollow silica cubes in crystalline films were reported by Meijer et al. [19] Detailed stacking were determined by scanning electron microscopy and small-angle X-ray scattering. Magnetic cubes and superballs of different experimental origin have been synthesized and their properties in solution been determined and complemented by simulation studies. For example, Kovalenko et al. [20] synthesized magnetite cubes of ca. 20 nm size from iron oleate precursors, Rossi et al. [18] and Wetterskog et al. [21] synthesized hematite superballs of ca. 1.0 μm size used ferric hydroxide gel, and Aoshima et al. [22] used ferric chloride hexahydrate as precursors and various amount of oleic acid/oleate to synthesize iron oxide superballs of different shape.

Meijer et al. [23] have studied the sedimentation of hematite cubes and determined the crystal structure by X-ray diffraction. A more extended study of colloidal cubes were performed by Castillo et al. [24] Their study included hematite cubes and cubes stabilized by a protecting polymer layer. Subsequently, Castillo et al. [25] demonstrated that silica cubes containing hematite could enhance the degradation of organic dyes. A review on the self-assembly of colloids possessing novel shapes has been written by Sacanna et al. [26]

Moreover, experimentally Wetterskog et al. [21] found the appearance of porous bundles of cubes at weak external field and more compact ones at stronger external field. These

March 30, 15

findings were qualitatively supported by model simulation of cubes possessing a magnetic dipole in along the cube diagonal in a quasi-2d geometry. Vutukuri et al. [27] considered nearly perfect neighborite (NaMgF_3) cubes in an external field, and they found the formation of strings at low density and hexagonal and square structures at high density. Singh et al. [28] demonstrated that helical superstructures could be developed, and they inferred the development of these structures as an interplay of van der Waals, magnetic dipole–dipole, and dipole–external field interactions by using simulation techniques. On the modelling side, Donaldson and Kantorovich [29] very recently performed a study of the ground states of clusters of magnetic cubes containing up to ca. 20 cubes.

The direction of the dipole moment of the magnetic superballs formed by hematite is yet not settled. It has been proposed that the direction is perpendicular to the space diagonal of the superball. [30] Even so, the angular distribution about that direction is yet unknown. With this background, the current work is centred around the question: *how is the structure of fluids of dipolar superballs affected by the direction of their dipoles?* In the following, (i) interaction energies between pairs of dipolar superballs at different configurations and (ii) results from Monte Carlo simulations of quasi-2d fluids of dipolar superball without and with the presence of an external field are presented for three different directions of the dipole. The dipole strength has been chosen such that the transition from a disordered to ordered fluids is covered. Systems with higher superball concentration approaching the crystal state will be considered in a subsequent publication.

The paper is organized as follows. The model and methods used are presented in Sec. 2. Section 3 contains our results. Results of the interaction of two dipolar particles at different configurations are given in Sec. 3.1. In this section, the interaction energy for different representation of the dipole moment is also compared. That is followed in Sec. 3.2 by an account of the results of the Monte Carlo simulations of dipolar superball fluids. In Sec. 4, the results are discussed with a particular emphasis on the role of the direction of the dipole in the superball. Finally, the paper ends with conclusions given in Sec. 5.

2 Model and methods

2.1 Model

Our model system is composed of N particles with an external homogeneous (magnetic) field potentially applied. The particles attain the shape of superballs and possess a central (magnetic) point dipole μ . Three-dimensional superballs are defined by points (x', y', z') fulfilling in inequality

$$|x'/R|^{2q} + |y'/R|^{2q} + |z'/R|^{2q} \leq 1 \quad (1)$$

in a *particle* coordinate frame with the parameter q describing its shape and R the center-to-surface distance of a cord along a principle axis of the superball. In particular, superballs becomes spheres at $q = 1$ with $2R$ being the diameter of the sphere and cubes in limit $q \rightarrow \infty$ with $2R$ being the length of a cube side. A superball with $q \neq 1$ belongs to the point group O_h and possesses 3 four-fold, 4 three-fold, and 6 two-fold axes. We will later see that the interplay between the different symmetries of a cube and of the dipole field is essential for understanding properties of the model system.

The total interaction energy U of the model system can be written as

$$U = U_{\text{part}} + U_{\text{ext}} \quad (2)$$

where U_{part} denotes the interaction energy among the particles and U_{ext} the interaction between the particles and the external field. The former is given as a sum of terms according to

$$U_{\text{part}} = \sum_{i < j} u(\mathbf{r}_{ij}, \Omega_i, \Omega_j) \quad (3)$$

where $u(\mathbf{r}_{ij}, \Omega_i, \Omega_j)$ denotes the pair interaction energy between particles i and j , and the latter as a single sum

$$U_{\text{ext}} = \sum_i u_{\text{ext}}(\boldsymbol{\mu}_i, \mathbf{B}_{\text{ext}}) \quad (4)$$

where $u_{\text{ext}}(\boldsymbol{\mu}_i, \mathbf{B}_{\text{ext}})$ denotes the interaction between particle i and the homogeneous external field \mathbf{B}_{ext} . Here, and in the following, \mathbf{r}_{ij} denotes the center-of-mass (com) – center-of-mass vector between particle i and j given by $\mathbf{r}_{ij} \equiv \mathbf{r}_i - \mathbf{r}_j$ with \mathbf{r}_i being the location of the center of particle i , center Ω_i specifying the orientation of the coordinate frame of particle i , and $\boldsymbol{\mu}_i$ the dipole moment of particle i , all with respect to an external coordinate frame. The pair interaction energy $u(\mathbf{r}_{ij}, \Omega_i, \Omega_j)$ entering in eqn (3) can be divided into two terms according to

$$u(\mathbf{r}_{ij}, \Omega_i, \Omega_j) = u_{\text{HC}}(\mathbf{r}_{ij}, \Omega_i, \Omega_j) + u_{\text{dip}}(\mathbf{r}_{ij}, \boldsymbol{\mu}_i, \boldsymbol{\mu}_j) \quad (5)$$

where the short-range hard-core interaction energy $u_{\text{HC}}(\mathbf{r}_{ij}, \Omega_i, \Omega_j)$ is given by

$$u_{\text{HC}}(\mathbf{r}_{ij}, \Omega_i, \Omega_j) = \begin{cases} \infty, & \text{superballs } i \text{ and } j \text{ are overlapping} \\ 0, & \text{superballs } i \text{ and } j \text{ are not overlapping} \end{cases} \quad (6)$$

and the long-range dipole-dipole interaction energy $u_{\text{dip}}(\mathbf{r}_{ij}, \boldsymbol{\mu}_i, \boldsymbol{\mu}_j)$ by

$$u_{\text{dip}}(\mathbf{r}_{ij}, \boldsymbol{\mu}_i, \boldsymbol{\mu}_j) = \frac{\mu_0}{4\pi} \left[\frac{\boldsymbol{\mu}_i \cdot \boldsymbol{\mu}_j}{r_{ij}^3} - 3 \frac{(\boldsymbol{\mu}_i \cdot \mathbf{r}_{ij})(\boldsymbol{\mu}_j \cdot \mathbf{r}_{ij})}{r_{ij}^5} \right] \quad (7)$$

with μ_0 being the permeability in vacuum. The interaction between particle i and the external field $u_{\text{ext}}(\boldsymbol{\mu}_i, \mathbf{B}_{\text{ext}})$ entering in eqn (4) is given by

$$u_{\text{ext}}(\boldsymbol{\mu}_i, \mathbf{B}_{\text{ext}}) = -\boldsymbol{\mu}_i \cdot \mathbf{B}_{\text{ext}} \quad (8)$$

Thus, u_{ext} depends on the orientation of the dipole with respect to the external field but not on the position of the dipole.

In the following, dimensionless units as defined in Table 1 will be used. The dimensionless dipole-dipole interaction energy becomes

$$u_{\text{dip}}^*(\mathbf{r}_{ij}^*, \boldsymbol{\mu}_i^*, \boldsymbol{\mu}_j^*) \equiv u_{\text{dip}}(\mathbf{r}_{ij}, \boldsymbol{\mu}_i, \boldsymbol{\mu}_j)/(kT) = \frac{\boldsymbol{\mu}_i^* \cdot \boldsymbol{\mu}_j^*}{(r_{ij}^*)^3} - 3 \frac{(\boldsymbol{\mu}_i^* \cdot \mathbf{r}_{ij}^*)(\boldsymbol{\mu}_j^* \cdot \mathbf{r}_{ij}^*)}{(r_{ij}^*)^5} \quad (9)$$

and the dimensionless dipole–external field interaction energy

$$u_{\text{ext}}^*(\boldsymbol{\mu}_i^*, \mathbf{B}_{\text{ext}}^*) \equiv u_{\text{ext}}(\boldsymbol{\mu}_i, \mathbf{B}_{\text{ext}})/(kT) = -\boldsymbol{\mu}_i^* \cdot \mathbf{B}_{\text{ext}}^* \quad (10)$$

where k is Boltzmann constant and T the temperature. Moreover, the dimensionless dipole-dipole coupling parameter

$$\lambda \equiv \frac{\mu_0}{4\pi} \left[\frac{\mu^2}{\sigma^3} \right] \quad (11)$$

with $\sigma = 2R$ and the dimensionless dipole–external field coupling parameter

$$\xi \equiv \frac{\mu_0}{4\pi} \mu B \quad (12)$$

are related to the dimensionless dipole strength μ^* and the dimensionless field strength B^* according to

$$\lambda \equiv (\mu^*)^2 \quad (13)$$

and

$$\xi \equiv \mu^* B^* \quad (14)$$

respectively. For simplicity, the word “dimensionless” we will from here be omitted.

2.2 Method

The quasi-2d fluid of superballs has been subjected to canonical Metropolis Monte Carlo simulation in a quasi-2d confinement with periodic boundary conditions applied in two directions. The surface of a superball was tiled using up to 4000 triangles and examination of superball overlap was performed by using a fast triangle-triangle intersection-test algorithm by Möller [31]. The Ewald sum is used for the long-range dipole–dipole interaction [32]. A combination of trial moves involving single-particle moves and cluster moves are used [33]. Equilibration involving 10^5 trial moves per particle (pass) has preceded the production run also comprising 10^5 passes. The average root-mean-square displacement of the superballs during the production run amounts to 32 to 300; cf. the box length of ca. 40.

2.3 Systems

We consider two types of model systems: (i) $N = 2$ dipolar superballs for different values of the shape parameter q , referred to as a two-particle system; and (ii) $N = 250$ dipolar superballs with $q = 1.5$ localized to the xy -plane of a 3d-space and confined within a quadratic area A but still retaining full 3d rotational ability, referred to as a quasi-2d system. The two-particle system is used to investigate the interaction between two dipolar superballs of different shape and the approximation of a homogeneous dipole density with a single dipole. The quasi-2d system is employed for studying the properties of quasi-2d fluids of dipolar superballs. A complete study with $N = 125$ of dipolar superballs and selected simulations with

$N = 500$ dipolar superballs displayed essentially the same results as with the $N = 250$ dipolar superballs used.

In both types of model systems, three different directions of the dipole moment with respect to the principal axes of the superbball are considered. The directions are (i) $\hat{\mu}' = (0, 0, 1)$, referred to as the 001-direction, and agree with a four-fold axis; (ii) $\hat{\mu}' = \frac{1}{\sqrt{2}}(0, 1, 1)$, referred to as the 011-direction, and agree with a two-fold symmetry axis; and (iii) $\hat{\mu}' = \frac{1}{\sqrt{3}}(1, 1, 1)$, referred to as the 111-direction, and agree with a three-fold symmetry axis. Fig. 1 illustrates the shape of a superbball with $q = 1.5$ and the three directions of the dipole moment chosen. In the limit of a cube, the three dipole moments become perpendicular to a surface, pass an edge, and pass a corner, respectively, of the cube.

For the quasi-2d systems, we have considered the four different dipole strengths $\mu^* = 1.86, 2.24, 2.61, 2.98$ at the external field $\mathbf{B}_{\text{ext}}^* = (0, 0, 0)$ and $(0.632, 0, 0)$, the latter implying a nonzero field parallel to the plane of particles. Further quantitative specifications of the quasi-2d systems are given in Table 1.

3 Results

3.1 Interaction energy between two dipolar particles

The understanding of the interaction between two superballs with a central, point dipole (referred to as dipolar superballs) facilitates the interpretation of the structure of dipolar superbball fluids. In this section, we will consider the interaction between two dipolar superballs with unit dipole moment ($\mu^* = 1$), preceded by the two limiting cases $q = 1$ (dipolar spheres) and $q \rightarrow \infty$ (dipolar cubes).

3.1.1 Dipolar spheres. Since the short-range interaction of a sphere is isotropic, only the dipole-dipole interaction contributes to the anisotropy of the interaction between two dipolar spheres. From eqn (7), it follows that the global interaction energy minimum with $U^* = -2$ appears at hard-sphere contact where the two dipoles are collinear with a head-to-tail arrangement. Local energy minima with $U^* = -1$ appear for antiparallel, side-by-side dipole arrangements at hard-sphere contact.

3.1.2 Dipolar cubes. The interaction between two dipolar cubes is more complex, originating from the disparate symmetry of a cube and the field of a dipole. Their different symmetries cause (i) an infinite number of unique orientations of the dipole vector with respect to the shape of the cube and (ii) a different orientational dependence of the short-range cube-cube interaction and of the dipole-dipole interaction.

The relative position and orientation (later referred to as configuration) of two dipolar cubes at their global interaction minimum for dipoles in the 001-, 011-, and 111-directions are shown in Fig. 2 (left column). Throughout, the global energy minima appear for side-by-side configurations of the two cubes. For dipoles in the 001-direction, the two dipoles in the two cubes are collinear and arranged head-to-tail, as for two dipolar spheres. However, for the 011- and 111-directions the situation becomes different. The global interaction minima still appear for closest dipole-dipole separation possible, implying that the dipoles here are not collinear or even parallel. For the 011-direction the dipole-dipole angle become $\arccos(0) = 90^\circ$ and the interaction energy $U^* = -3/2$, and for the 111-direction we get $\arccos(-1/3) \approx 109^\circ$ and $U^* = -4/3$, respectively. Obviously, the collinear arrangement appearing for dipolar spheres has to yield for the short-range cube-cube interaction for dipoles in the 011- and 111-directions. Thus, an origin for a richer behavior for dipolar cubes as compared to a dipolar spheres can be anticipated.

The presence of a homogeneous external field tends to aline the directions of dipoles. Therefore, it is also of interest to examine minimum interaction energies of two dipolar cubes and corresponding configurations under the constraint of *parallel* dipole directions. Fig. 2 (middle column) displays such configurations and minimum interaction energies for the three different dipole directions. Corresponding energetic data under the even more severe constraint of *collinear* dipoles are also given in Fig. 2 (right column).

For the 001-direction, the configurations under the constraint of parallel dipoles and of collinear dipoles are identical with that of the global energy minimum, since the latter exhibits collinear dipoles. For the 011- and 111-directions, the energy minimum under the constraint of parallel dipole directions appears for a configuration described as a side-by-side arrangement with parallel dipoles followed by a translational shift of one of the cubes in the direction of the dipoles. For the 011-direction, the shift is 0.43 giving a configuration (see Fig. 2, middle row, middle column) with an interaction energy $U^* \approx -1.23$. This could be compared with the interaction energy $U^* = -1/\sqrt{2} \approx -0.71$ for an edge-to-edge configuration with collinear dipoles. Finally, for the 111-direction a shift of 0.55 giving a configuration (see Fig. 2, bottom row, middle column) an interaction energy $U^* \approx -0.96$. The corner-to-corner configuration with collinear dipoles has the interaction energy $U^* = -2/(3\sqrt{3}) \approx -0.38$.

Noticeable, for dipoles in the 011-direction under the constraint of parallel dipoles the configuration of the energy minimum possesses a two-folded degeneration, and for the 111-

March 30, 15

direction a three-folded degeneration. At the condition of collinear dipoles, this structural degeneration vanishes.

To conclude: (i) The strongest interaction between two dipolar cubes appears for dipoles in the 001-direction and a configuration where the two dipoles are head-to-tail aligned. An external field does not compromise this conformation. (ii) Conformations with less negative interaction minima appear for the 011- and 111-directions. An external field affects these conformations, and both their interaction minima are attenuated.

3.1.3 Dipolar superballs. We will now consider interaction energy minima for a pair of dipolar superballs. Energy minima and corresponding structures of two dipolar superballs at different values of the shape parameter q were determined by simulated annealing. For each case, simulated annealing was performed with two different start configurations of the dipolar superballs: (i) global energy-minimum configurations and (ii) collinear head-to-tail configurations with the superballs being in contact. For the 011- and 111-directions, these two start configurations lie in two different interaction-energy wells. The annealing protocol was chosen such that the structures remained in the energy well of its start configuration by selecting low temperature and small displacement parameters. Hence, the annealing process just brings the dipolar superballs from the start configuration to their closest energy minimum, and no crossing of the energy barrier between the two energy wells appear.

The resulting energy minimum as a function of the shape parameter q as well as the limiting energy values for dipolar cubes for the three dipole directions are given in Fig. 3. For all three dipole directions, the expected minimum energy $U^* = -2$ for spheres ($q = 1$) was trivially obtained. Similarly, same minimum energy was obtained for dipoles in the 001-direction for all values of the shape parameter of the superball considered. However, for the 011- and 111-directions, a transition from configurations with parallel dipoles to ones with nonparallel dipoles occurred. The transition appeared at $q' \approx 1.35$ and the interaction energy $U^* = -1.60$ for the 011-direction and at $q' \approx 1.30$ and $U^* = -1.40$ for the 111-direction. At $q > q'$, the interaction energy of the nonparallel configurations decreases only slowly at increasing q , and in the limit of dipolar cubes the interaction energy attains the values $U^* = -3/2$ and $U^* = -4/3$ for the 011- and 111-directions, respectively.

In the following, focus will be on superballs with a shape parameter $q = 1.5$. From Fig. 3, we notice minimum interaction energies $U^* = -1.55$ for the 011-direction and $U^* = -1.37$ for the 111-direction for nonparallel dipoles. Hence, the strength of the pair interaction of two dipolar superballs decreases in the order 001-, 011-, and 111-direction with the dipoles collinear for the 001-direction and nonparallel for the 011- and 111-directions. In the case of

parallel dipole directions, e.g., forced by a strong external field, the interaction energies rise to $U^* = -1.45$ and $U^* = -1.20$ for the 011- and 111-directions, respectively. Thus, the order of the interaction strength among the three dipole directions is preserved in the presence of a strong external field.

3.1.4 Interaction energy for different representation of the magnetization. So far, we have represented the dipolar density of the particles with a central, point dipole. However, a homogeneous dipole density is a better representation of single-crystal magnetic particles. [1] Thus, the single-dipole description constitutes a simplification. In this section, this simplification will be examined for the cases given in Fig. 2 using (i) a multisite and (ii) a multipole expansion. Again we will consider cubes with a unit dipole moment.

A multisite expansion constitutes an improved description of a homogeneous magnetization of a cube. Such an expansion involved a division of the dipolar cube into p^3 equal cubes on a primitive cubic lattice and assigning a central, point dipole with a dipole moment p^{-3} to each of the p^3 cubes, Fig. 4 provides the normalized interaction energy $U_p^*/U_{p=1}^*$ of two cubes as a function of $1/p$, $p = 1-4$, for the configurations given in Fig 2. An extrapolation to $p \rightarrow \infty$, suggests that the improved description reduces the magnitude of the interaction energy for configurations at the global interaction energy minimum. Also the configurations with parallel dipoles display a reduced magnitude of the interaction energy; here the reduction of the normalized interaction energy is even larger, ca. 10-20 %. However, the reductions diminish rapidly with increasing cube separation and are negligible at $r^* \geq 1.3$. Hence, we conclude that the simplified representation of a cube with a homogeneous dipole density with a single point dipole can overestimate the dipole-dipole interaction between two such cubes at contact by 10-20 %. As the overestimate decays quickly with increasing separation, the overall effect becomes density dependent. Previously, Okada et al. [34] have demonstrated a weaker attraction obtained for a delocalized dipole distribution, as compared to a single, central one, by for platelets with an in-plane dipole direction.

A multipole expansion, comprising multipoles with only nonzero odd moments in the center of the cube, constitutes another formally exact representation of a homogeneous magnetization of a cube. In this representation, the interaction between two cubes with a homogeneous dipole density is given by the interaction between two multipoles. In our application with superballs with a shape parameter $q = 1.5$, this approach does not hold for some configurations of nearby superballs. Nevertheless, a multipole expansion of the magnetization may still be viable in simulations of models beyond a central, point dipole, if

the expansion is augmented with an explicit multisite summation for those configurations where the multipole expansion is invalid or very slowly convergent.

3.2 Quasi-2d fluids

Energetics and structural properties have been determined for quasi-2d fluids of dipolar superballs possessing a shape parameter $q = 1.5$ for dipoles oriented in the 001-, 011-, and 111-directions. The structure of the quasi-2d fluids has been characterized qualitatively by snapshots and quantitatively by distribution functions. Examination has been made for four dipole strengths without and with a homogeneous field applied parallel to the plane of the superballs.

3.2.1 Interaction energy. Ensemble-averaged particle–particle interaction energy per particle $\langle U_{\text{part}}^* \rangle / N$ and corresponding particle–external-field interaction energy $\langle U_{\text{ext}}^* \rangle / N$ as a function of the dipole strength μ^* are provided in Fig. 5. We observe the following:

- (i) For the smallest dipole strength, $\mu^* = 1.86$, the magnitude of both $\langle U_{\text{part}}^* \rangle / N$ and $\langle U_{\text{ext}}^* \rangle / N$ is less than 2.
- (ii) The magnitude of $\langle U_{\text{part}}^* \rangle / N$ increases superlinear with μ^* , whereas the magnitude of $\langle U_{\text{ext}}^* \rangle / N$ increases nearly linearly at increasing μ^* .
- (iii) The magnitude of $\langle U_{\text{part}}^* \rangle / N$ increases with μ^* faster in the presence of the external field than in the absence of it.
- (iv) In all cases, the magnitude of the interaction energy is largest for dipoles in the 001-direction and smallest for the 111-direction with the difference between the 011- and 111-directions being smaller.

Hence, we cover the interesting range where energetics varies between $O(1)$ to $O(10) kT$ per particle with clear differences between the different dipole directions.

3.2.2 Snapshots. Snapshots taken at the end of the production simulations are provided in Figs. 6-8 for dipoles in the 001-, 011-, and 111-directions, respectively, at the dipole strengths $\mu = 1.86, 2.24, 2.61, 2.98$ without and with an external field applied. The following is observed for all the three dipole directions:

- (i) The dipolar superball fluid becomes progressively more ordered at increasing dipole strength.
- (ii) At the smallest dipole strength, $\mu = 1.86$ the fluid becomes orientationally weakly ordered but remains translationally disordered when the external field is applied.

- (iii) At the largest dipole strength, $\mu^* = 2.98$, the superballs form 1d aggregates (chains); the chains are curved and sometimes closed without an external field and linear in the field direction with the external field applied.

Upon a closer inspection, we discern the following differences among the three different dipole directions:

- (iv) The onset of chain formation appears at lower dipole strength μ^* for the 001-direction as compared to the 011- and 111-directions.
- (v) At the smallest dipole strength, $\mu^* = 2.98$, and no external field applied, no bifurcation (four-way junction) appears for dipoles for the 001-direction, whereas bifurcations appear for the 011- and 111-directions. The number of bifurcations increases, making the chains and loops smaller in the sequence 011-direction and 111-direction (Figs. 6-8, top-left panel).
- (vi) At the smallest dipole strength, $\mu^* = 2.98$, and with external field applied, the linear chains are separated for dipoles in the 001-direction and bundled for the other two dipole directions. The frequency of chain bundling increases in the sequence 011-direction and 111-direction (Figs. 6-8, top-right panel, insert).

Thus, for the chosen area density the selected set of dipole strengths covers a transition (i) from a disordered fluid of separated superballs (ii.a) to an isotropic fluid of chains and loops of superballs in the absence of an external field and (ii.b) to an anisotropic fluid of individual or bundled chains of superballs in the presence of an external field parallel to the plane of the superballs. These features appear for all three directions of the dipole moment of the superballs, though some significant differences remain.

3.2.3 Distribution functions. The translational structure of the superball fluids has been quantified by the cluster size probability function $P(n)$ and the 2d radial distribution function $g(r^*)$. Two superballs directly or indirectly being separated by $r^* \leq 1.3$ are considered to belong to the same cluster. The separation r^* corresponds to, or is near, the first minimum of the radial distribution function (see Fig. 10 below). The outcome of the cluster analysis is insensitive on the exact value of r^* . The orientational order of nearby superballs was examined by the dipole–dipole angular probability function $P(\hat{\mu}_i \cdot \hat{\mu}_j)$ and the dipole–com-vector angular probability function $P(\hat{\mu}_i \cdot \hat{\mathbf{r}}_{ij})$. Two superballs are nearby when separated $r^* \leq 1.3$. Finally, the orientation in the presence of the external field has been characterized by the dipole–external-field angular probability function $P(\hat{\mu}_i \cdot \hat{\mathbf{z}})$. In the following selected

distribution functions of the 24 systems will be presented to quantify the most important structural features.

The distribution of clusters with n superballs $P(n)$ for selected values of the dipole strength are shown in Fig. 9. At the two lower dipole moments, where the probability of larger clusters is small, the probability distribution is basically logarithmically decaying, except for $\mu^* = 2.24$ for the 001-direction in the presence of the external field. Without an external field, the fraction of nonclustered (isolated) superballs at the dipole strength $\mu^* = 2.24$ is 0.16, 0.26, 0.28 and at the dipole strength $\mu^* = 2.61$ is 0.0, 0.04, 0.06 for the 001-, 011-, and 111-directions of the dipoles, respectively (Fig. 9a). In the presence of the external field, (i) precisely the same ordering among the three dipole directions appear and (ii) the fractions of nonclustered dipoles are in all cases lower than those at zero external field (Fig. 9b). Hence, the degree of nonclustered superballs increases in the order 001-, 011-, and 111-directions and decreases in the presence of an external field.

Selected 2d radial distribution functions $g(r^*)$ are displayed in Fig. 10. The typical increase of the structure at increasing dipole strength μ^* is evident by (i) the sharpening and (ii) the more numerous peaks at $r^* \approx n$, $n = 1, 2, 3, \dots$ for systems with dipoles in the 001-direction in the absence of the external field (Fig. 10a). For the most ordered system, spatial correlations extend ≈ 10 particle-layers away. For the largest dipole strength $\mu^* = 2.98$, it is clear that the spatial correlations becomes less prominent in the order 001-, 011-, and 111-directions of the dipoles and increases with the external field applied (Fig. 10b).

Fig. 11 displays dipole–dipole angular probability functions $P(\hat{\mu}_i \cdot \hat{\mu}_j)$ for nearby superballs. All distribution functions display their global maximum at $\theta = \arccos(1) = 0^\circ$ corresponding to a parallel, attractive head-to-tail dipole-dipole arrangement. We notice that the alignment of the dipole directions increases sharply with increasing dipole strength for the 011-direction (Fig. 11a) and that the tendency of alignment is strongly reduced in the order 001-, 011-, and 111-directions of the dipoles and substantially enhanced in the presence of the external field (Fig. 11b).

Dipole–com-com-vector angular probability functions $P(\hat{\mu}_i \cdot \hat{r}_{ij})$ are presented in Fig. 12. All distribution functions posses expected inversion symmetry and maxima at $\theta = 0^\circ$ and 180° . The qualitative dependences on μ_i^* and B_x^* are the same as for the dipole–dipole angular probability functions. Though the minima of $P(\hat{\mu}_i \cdot \hat{\mu}_j)$ is smaller than those of $P(\hat{\mu}_i \cdot \hat{r}_{ij})$, as expected for the dipolar interaction, the maximal values of $P(\hat{\mu}_i \cdot \hat{\mu}_j)$ and $P(\hat{\mu}_i \cdot \hat{r}_{ij})$ are similar. In the absence of a field, we notice a weak local maxima of $P(\hat{\mu}_i \cdot \hat{r}_{ij})$ for $|\hat{\mu}_i \cdot \hat{r}_{ij}| \approx$

0.45. This implies a low appearance of parallel chains displaced by $r^* = 1$, also observed for dipolar spheres. [6] Moreover, the $P(\hat{\mu}_i \cdot \hat{r}_{ij})$ probability displays a weaker dependence on the external field as compared to $P(\hat{\mu}_i \cdot \hat{r}_{ij})$ (cf. Fig. 12b with Fig 11b), as expected.

Finally, Fig. 13 displays the dipole–external-field angular probability function $P(\hat{\mu}_i \cdot \hat{z})$ for superballs with dipoles in the 001-direction. Note, the z-axis is perpendicular to the field direction. The maximum of $P(\hat{\mu}_i \cdot \hat{z})$ appears at $\hat{\mu}_i \cdot \hat{z} = 0$, corresponding to a direction perpendicular to the z-axis. Hence, the dipoles are preferentially oriented in the direction of the external field. The distribution is broad at small dipole strength, and it sharpens at increasing dipole strength. The distributions across 001-, 011-, and 111-directions (data not shown) are very similar with slightly more peaked distributions for the 001-direction.

4 Discussion

We are now at the position to combine and discuss our energetic and structural observations (i) of the quasi-2d systems given in Sec. 3.2 and with those of the two-particle system described in Sec. 3.1. As alluded to in the introduction, the dissimilarities obtained for the different directions of the dipole with respect to the shape of the superball are of particular interest.

(A) For the dipolar strength $\mu^* = 1.86$, the appearance of disordered fluids (Figs. 6-8, bottom) is consistent with a dipole-dipole interaction energy of the order of $1-2kT$ (Fig. 5). Hence, the dipolar interaction energy among the superballs is too weak, as compared to the thermal energy, to establish any long-range order. Furthermore, the chain formation appearing at the dipole strength $\mu^* = 2.98$ (Figs. 6-8, top) is also consistent with the dipolar interaction energy, now $>10kT$ (Fig. 5). Since superballs in chains are linked to at most two neighbors, the dipole-dipole interaction energy between two neighboring superballs exceeds the thermal energy 5-fold.

(B) Orientationally alignment of the superballs by the external field is visible already at the dipolar strength $\mu^* = 1.86$ (Figs. 6-8 bottom-right panel, insert) and is quantified by the dipole–external-field angular probability function (Fig. 13). These observations are consistent with the external energy of $\approx 2kT$ (Fig. 5) at this dipolar strength.

(C) We noticed that the dipole–dipole interaction energy becomes more negative in the presence of the external field (Fig. 5). This is a consequence of the orientational alignment of the dipoles by the external field leading to a *reduced* orientational disorder, which in turn facilitates a favorable dipole-dipole interaction and chain formation. However, with the

March 30, 15

external field applied the dipole-dipole interaction has yet to overcome the translational disorder, which is not primarily affected by the dipole–external-field interaction.

(D) As compared to the 011- and 111-directions, we connect the onset of chain formation appearing at lower dipole strength for 001-directions (Figs. 6-8) with the stronger pair interaction of two dipolar cubes with dipoles in the 001-direction appearing both without any constraint of their dipole directions (Fig. 2, left column) and with enforced dipole directions appearing in a strong external field (Fig. 2, middle column).

(E) The increased bundling appearing in the sequence 001-, 011-, and 111-direction for large dipole moments in the presence of the external field (Figs. 6-8, top-right panel, insert) is attributed to the two-fold and three-fold degeneration of the minimum energy configuration of the 011- and 111-directions under the constraint of parallel dipole directions (Fig. 2 and related discussion).

Hence, the different symmetry of a cube and of a dipole field gives rise to no energy frustration for dipoles in the 001-direction and energy frustration for dipoles in the 011- and 111-directions of two nearby superballs with $q = 1.5$. This frustration will be reduced at smaller values of q , for which a superball deviates less from a sphere. Obviously, the three different dipole orientations degenerate in the limit of a sphere ($q = 1$).

Despite the different scope of the current and the previous [29] studies, the models used display similarities. Donaldson and Kantorovich considered dipolar cubes composed by fused spheres, also in a quasi-2d geometry. The number of spheres representing the cubes was sufficiently large to isolate the effect of the overall cubic shape and the surfaces roughness. In their study, they considered the ground-state configuration (conformations possessing the lowest interaction energy at $T = 0$) for cluster containing up ca. 20 dipolar cubes possessing dipoles either in the 001- or the 111-direction in the absence of an external field. Their and our findings of the ground state of $N = 2$ clusters for the two dipolar directions agree. Moreover, for larger N they demonstrated the appearance of more complicated ground states for dipoles in the 111-direction. The richer behavior for the 111-direction, as compared to dipoles in the 001-direction, shown by Donaldson and Kantorovich at $T = 0$ and here at higher temperature in the absence and in the presence of an external field, have the same origin; viz. different cube and dipole-interaction symmetry.

Finally, we will now return to experimental work on magnetic superballs made by hematite in the presence of an external magnetic field. Currently, the direction of the dipole with respect to the shape of the cube is not yet settled. Arguments have been given for a direction perpendicular to the space diagonal [30], but a space diagonal dipole direction has

also been employed in modelling hematite cubes. [22] In the former case, the distribution around the diagonal axis is yet unknown – do we have a random distribution or is some direction preferred? Nevertheless, the 011-direction considered in this contribution is consistent with some of the dipole direction perpendicular to the space diagonal, whereas the 001- and 111-directions are not. Though clear different structures obtained for the different dipole directions, the results from the present work is not sufficient at the present time to shed further light on the dipole direction(s) of cubic hematite, it is envisioned that further simulation studies at higher densities, including crystalline structures, are required to provide improved insight into the direction(s) of the magnetic moment of cubic particles formed by hematite.

4 Conclusions

Model investigations have been performed on the interaction between two dipolar superballs and 2d-fluids of superballs. Different directions of the dipole with respect to the shape of the superball have been employed. Different dipole moments corresponding to disordered fluids as well as fluids containing string-like dipole chains have been used, and the influence of an external field parallel to the fluid plane has also been considered.

Under appropriate conditions, the dipolar superballs formed strings when the dipole moment exceeds a threshold value. This threshold of the dipole moment increases in the sequence of 001-, 011-, and 111-directions and reduces slightly when the external field is applied. In the absence of an external field, strings are curved and form bifurcations for the 011- and 111-directions, whereas in the presence of the field, the strings are straight and aligned with bundle formation appearing for dipoles the 011- and 111-directions.

The origin of

- (A) the larger threshold for string formation,
- (B) increased bifurcations, and
- (C) increased bundle formation for the 011- and 111-directions

as compared to the 001-direction lies in direction of the dipole moment with respect to the shape of the superball. For the 001-direction, the global energy minimum appears for dipoles collinearly arranged and at the shortest cube-cube separation. The global energy minimum is energetically well separated from other local energy minima. On the contrary, for the 011- and 111-directions the global interaction energy minimum appears for superballs in surface-to-surface contact with nonparallel dipole arrangement. Other local energy minima with parallel dipoles are energetically close, implying several contact configurations with small

March 30, 15

energy differences. The effect of the field from other dipoles and of an external field parallel to the superball plane favor the parallel dipole orientations and suppresses the appearance of the global energy minimum configuration having nonparallel dipole orientation.

The present investigation of quasi-2d superball fluids has been focused a single shape parameter and at one number density of the superballs. In future studies, we will expand our study and make detailed comparison with experimental data on hematite superballs.

Acknowledgments

Björn Linse is gratefully acknowledged for implementing the tiling and triangle-triangle intersection-test algorithms and Albert Philipse for inspiring discussions on colloidal cubes. This work was supported by the Swedish Research Council (VR) through the Linnaeus grants for the Organizing Molecular Matter (OMM) center of excellence (239-2009-6794) and through an individual grant to P. L. (2010-2253-78321-47).

References

- [1] C. Holm and J.-J. Weis, *Curr. Opin. Colloid Interface Sci.* 2005, **10**, 133.
- [2] J. D. G. Durán, J. L. Arias, V. Gallardo and A. V. Delgado, *J. Phar. Sci.* 2008, **97**, 2948.
- [3] R. Ravaud, G. Lemarquand and V. Lemarquand, *J. Appl. Phys.* 2009, **106**, 034911.
- [4] S. F. Medeiros, A. M. Santos, H. Fessi and A. Elaissari, *Int. J. Pharm.* 2011, **403**, 139.
- [5] M. Bahiraei and M. Hangi, *J. Magn. Magn. Mater* 2015, **374**, 125.
- [6] J.-J. Weis, *Mol. Phys.* 2005, **103**, 7.
- [7] H. Schmidle, C. K. Hall, O. D. Velev and S. H. L. Klapp, *Soft Matter* 2012, **8**, 1521.
- [8] S. Kantorovich, R. Weeber, J. J. Cerda and C. Holm, *Soft Matter* 2011, **7**, 5217.
- [9] M. Piastra and E. G. Virga, *Soft Matter* 2012, **8**, 10969.
- [10] E. C. Gartland, Jr. and E. G. Virga, *Soft Matter*, 2013, **9**, 5991.
- [11] M. Klinkigt, R. Weever, S. Kantorovich and C. Holm, *Soft Matter*, 2013, **9**, 3535.
- [12] A. Abrikosov, S. Sacanna, A. P. Philipse and P. Linse, *Soft Matter*, 2013, **9**, 8904.
- [13] S. Sacanna, L. Rossi, and D. J. Pine, *J. Am. Chem. Soc.*, 2012, **134**, 6112.
- [14] R. D. Batten, F. H. Stillinger, and S. Torquato, *Phys. Rev. E.* 2010, **81**, 061105.
- [15] R. Ni, A. P. Gantapara, J. de Graaf, R. van Roij and M. Dijkstra, *Soft Matter*, 2012, **8**, 8826.
- [16] A. P. Gantapara, J. de Graaf, R. van Roij, and M. Dijkstra, *Phys. Rev. E*, 2013, **111**, 015501.

- [17] C. Knoroswki and A. Travasset, *J. Am. Chem. Soc.* 2014, 136, 653.
- [18] L. Rossi, S. Sacanna, W. T. M. Irvine, P. M. Chaikin, D. J. Pine, and A. P. Philipse, *Soft Matter*, 2011, 7, 4139.
- [19] J.-M. Meijer, F. Hagemans, L. Rossi, D. V. Byelov, S. I. R. Castillo, A. Snigirev, I. Snigireva, A. P. Philipse, and A. V. Petukhov, *Langmuir* 2012, 28, 7631.
- [20] M. V. Kovalenko, M. I. Bodnarchuk, R. T. Lechner, G. Hesser, F. Schäffler and W. Heiss, *J. Am. Chem. Soc.*, 2007, 129, 6352.
- [21] E. Wetterskog, M. Agthe, A. Mayence, J. Grins, D. Wang, S. Rana, A. Ahniyaz, G. Salazar-Alvarez and L. Bergström, *Sci. Technol. Adv. Mater.*, 2014, 15, 055010.
- [22] M. Aoshima, M. Ozaki and A. Satoh, *J. Phys. Chem. C*, 2012, 116, 17862.
- [23] J.-M. Meijer, D. V. Byelov, L. Rossi, A. Snigirev, I. Snigireva, A. P. Philipse, and A. V. Petukhov, *Soft Matter* 2013, 9, 10729.
- [24] S. I. R. Castillo, S. Ouhajji, S. Fokker, B. H. Ern , C. T. W. M. Schneijdenberg, D. M. E. Thies-Weesie, A. P. Philipse, *Microporous and Mesoporous Materials*, 2014, 195, 75.
- [25] S. I. R. Castillo, C. E. Pompe, J. van Mourik, D. M. A. Verbart, D. M. E. Thies-Weesie, P. E. de Jongh and A. P. Philipse *J. Mater. Chem. A*, 2014, 2, 10193.
- [26] S. Sacanna, D. J. Pine, and G.-R. Yi, *Soft Matter* 2013, 9, 8106.
- [27] H. R. Vutukuri, F. Smalenburg, S. Badaire, A. Imhof, M. Dijkstra and A. van Blaaderen, *Soft Matter*, 2014, 10, 9110.
- [28] G. Singh, H. Chan, A. Baskin, E. Gelman, N. Repnin, P. Kr l, and R. Klajn, *Science*, 2014, 345, 1149.
- [29] J. G. Donadson and S. S. Kantorovich, *Nanoscale*, 2015, 7, 3217.
- [30] L. Rossi, *Colloidal superballs*, Ph.D. Thesis, Utrecht University (2012).
- [31] T. M ller, *J. of Graph Tools*, 1997, 2, 25.
- [32] M. P. Allen and D. J. Tildesley, *Computer simulation of liquids*, Oxford University Press, 1987.
- [33] P. Linse In "Advanced computer simulation approaches for soft matter sciences II" Book series: "Advances in polymer science", Vol. 185, p 111. Eds: Holm, C. and Kremer, K. (Springer, Berlin, 2005).
- [34] I. Okada, M. Oazki, and E. Matijevic, *J. Colloid Interface Sci.* 1991, 142, 251.

March 30, 15

Table 1 Variables and values characterizing the fluid system investigated

Variable	Label	Value
number of particles	N	250
particle “radius”	R	
dimensionless distance	$r^* \equiv r/(2R)$	
box length	L	
box area	$A = L^2$	
dimensionless area	$\rho^* \equiv (N/A)(2R)^2$	0.15625 ¹
density		
shape parameter	q	1.5
dipole direction	$\hat{\mu}'$	$(0, 0, 1), \frac{1}{\sqrt{2}}(0, 1, 1), \frac{1}{\sqrt{3}}(1, 1, 1)$
dimensionless magnetic dipole	$\mu^* \equiv \left[\frac{\mu_0}{2\pi} (2R)^3 (kT)^{-1} \right]^{1/2}$	$\mu_1^* = 1.8635$ $\mu_2^* = 2.2362$ $\mu_3^* = 2.6089$ $\mu_4^* = 2.9816$
dimensionless external field	$\mathbf{B}_{\text{ext}}^* = (B_x^*, 0, 0)$ $\equiv \left[\frac{\mu_0}{2\pi} (2R)^3 (kT) \right]^{-1/2} \mathbf{B}_{\text{ext}}$	$B_{x,1}^* = 0$ $B_{x,2}^* = 0.6320$
dimensionless energy	$U^* \equiv U/(kT)$	

¹ For $q = 1$. Square length L and area A depends on q given a constant area fraction, see Table A2.

Appendix 1: Geometrical properties of a superball

A three-dimensional superball is defined by the points (x,y,z) satisfying the inequality

$$|x/R|^{2q} + |y/R|^{2q} + |z/R|^{2q} \leq 1 \quad (\text{A.1})$$

where q describes the shape and R the size of the superball. The shape parameter q transforms the superball continuously from a sphere at $q = 1$ to a cube in the limit $q \rightarrow \infty$. At $q = 1$ the parameter R becomes the radius of the sphere, and in the limit $q \rightarrow \infty$ the parameter R becomes the length of the cube edge.

The volume of a superball $v_{sb}(q)$ of unit radius ($R = 1$) is given by

$$v_{sb}(q) = \frac{2}{q^2} B\left(\frac{1}{2q}, \frac{2q+1}{2q}\right) B\left(\frac{1}{2q}, \frac{q+1}{q}\right) = \dots = \frac{2}{3q^2} \frac{\left[\Gamma\left(\frac{1}{2q}\right)\right]^3}{\Gamma\left(\frac{3}{2q}\right)} \quad (\text{A.2})$$

where $B(x, y) = \Gamma(x)\Gamma(y)/\Gamma(x+y)$ and $\Gamma(x)$ is the Euler gamma function. In particular, the volume $v_{sb}(q)$ divided by the volume of a sphere $v_{sb}(q = 1)$ becomes

$$\frac{v_{sb}(q)}{v_{sb}(q=1)} = \frac{1}{2\pi q^2} \frac{\left[\Gamma\left(\frac{1}{2q}\right)\right]^3}{\Gamma\left(\frac{3}{2q}\right)} \quad (\text{A.3})$$

The center-to-center distance d between two superballs in contact depends on (i) the relative orientations of the superballs and (ii) the shape parameter m . Contact distances for three relative orientations as a function of m are provided in Table A1.

Since the volume of a superball depends on m , either R or the confining volume V of a fluid of superballs has to vary with m to attain a fluid of constant volume fraction. For constant R , we have $V(q)/V(q = 1) = v_{sb}(q)/v_{sb}(q = 1)$. In particular for a confining cube, its edge length L becomes

$$\frac{L(q)}{L(q=1)} = \left[\frac{V(q)}{V(q=1)} \right]^{1/3} = \frac{\left[\Gamma\left(\frac{1}{2q}\right)\right]}{\left[2\pi q^2 \Gamma\left(\frac{3}{2q}\right)\right]^{1/3}} \quad (\text{A.4})$$

Some numerical values of $v_{sb}(q)$, $v_{sb}(q)/v_{sb}(q = 1)$, and $L(q)/L(q = 1)$ as a function of m are provided in Table A2.

March 30, 15

Table A1 Center-to-center separation d at close contact as a function of the shape parameter m for different relative orientations of two superballs normalized by the corresponding separation of two spheres $d(q = 1)$.

Relative orientation	$d(q)/d(q = 1)$
surface-to-surface	1
edge-to-edge	$2^{(1/2)(1-1/q)}$
corner-to-corner	$3^{(1/2)(1-1/q)}$

Table A2 Volume $v_{sb}(q)$ of superballs of unit radius at some values of the shape parameter q and relative volume $v_{sb}(q)/v_{sb}(q = 1)$ as well as and relative length of confining cube at constant volume fraction $L(q)/L(q = 1)$.

q	$v_{sb}(q)$	$v_{sb}(q)/v_{sb}(q = 1)$	$L(q)/L(q = 1)$
1	$4\pi/3$	1	1
1.5	5.6963	1.360	1.1079
2	6.4820	1.5475	1.1567

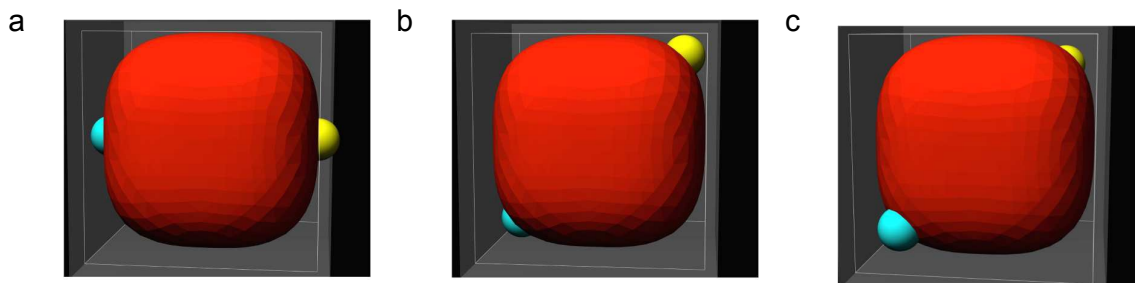


Fig. 1 Illustration of superballs possessing the shape parameter $q = 1.5$ and having a dipole moment in the (a) 001-direction, (b) 011-direction, and (c) 111-direction. The superballs are inscribed in cubes obtained in the limit $q \rightarrow \infty$. The yellow and blue spheres just indicate the dipole directions and no excluded volumes are associated with them.

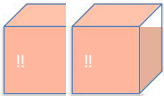
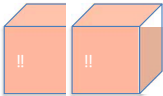
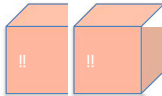
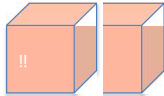
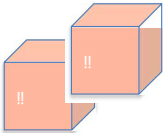
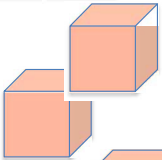
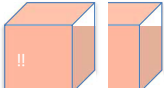
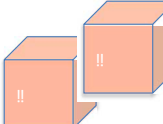
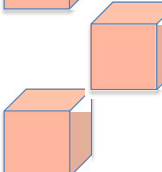
		Constraints				
		None	Parallel dipoles	Collinear dipoles		
001		<div>-2</div>		<div>-2</div>		<div>-2</div>
011		<div>$-\frac{3}{2}$</div>		<div>-1.23</div>		<div>$-\frac{2}{2\sqrt{2}}$</div>
111		<div>$-\frac{4}{3}$</div>		<div>-0.96</div>		<div>$-\frac{2}{3\sqrt{3}}$</div>

Fig. 2 Relative position and orientation of pairs of magnetic cubes and their interaction energy U^* for cubes possessing a central, unit dipole in the 001-, 011-, and 111-direction under the following constraints: none, parallel dipoles, and collinear dipoles.

March 30, 15

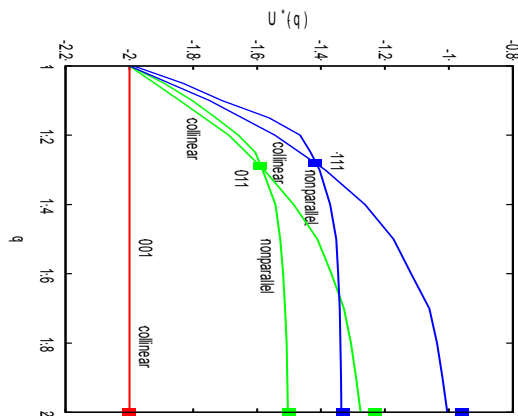


Fig. 3 Minimum interaction energy of two dipolar superballs U^* as a function of the shape parameter q for dipoles in the 001-direction at collinear configuration and for dipoles in 011- and 111-directions at collinear and nonparallel configurations. The collinear branch has lower interaction energy at small q and the nonparallel branch at large q . The corresponding energies for dipolar cubes ($q \rightarrow \infty$) are given by symbols located on the right ordinate.

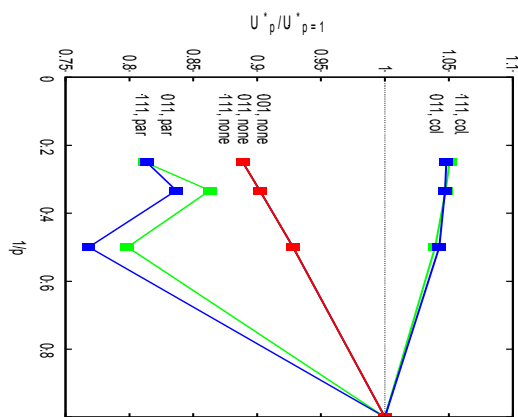


Fig. 4 Normalized interaction energy of two dipolar cubes $U_p^*/U_{p=1}^*$ as a function of $1/p$ for the configurations given in Fig. 2. A cube possesses unit side length and p^3 dipoles with dipole moment p^{-3} in the 001-, 011-, or 111-direction.

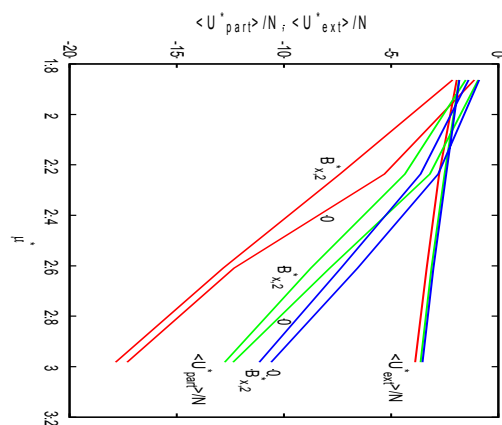


Fig. 5 Ensemble-averaged particle–particle interaction energy $\langle U^*_{part} \rangle / N$ (solid curves) and ensemble-averaged particle–external field interaction energy $\langle U^*_{ext} \rangle / N$ (solid curves) given per particle N as a function of the dipole strength μ^* for dipoles oriented in the 001-direction (red), 011-direction (green), and 111-direction (blue) at indicated strength of an external field B^*_x parallel to the plane of the superballs.

March 30, 15

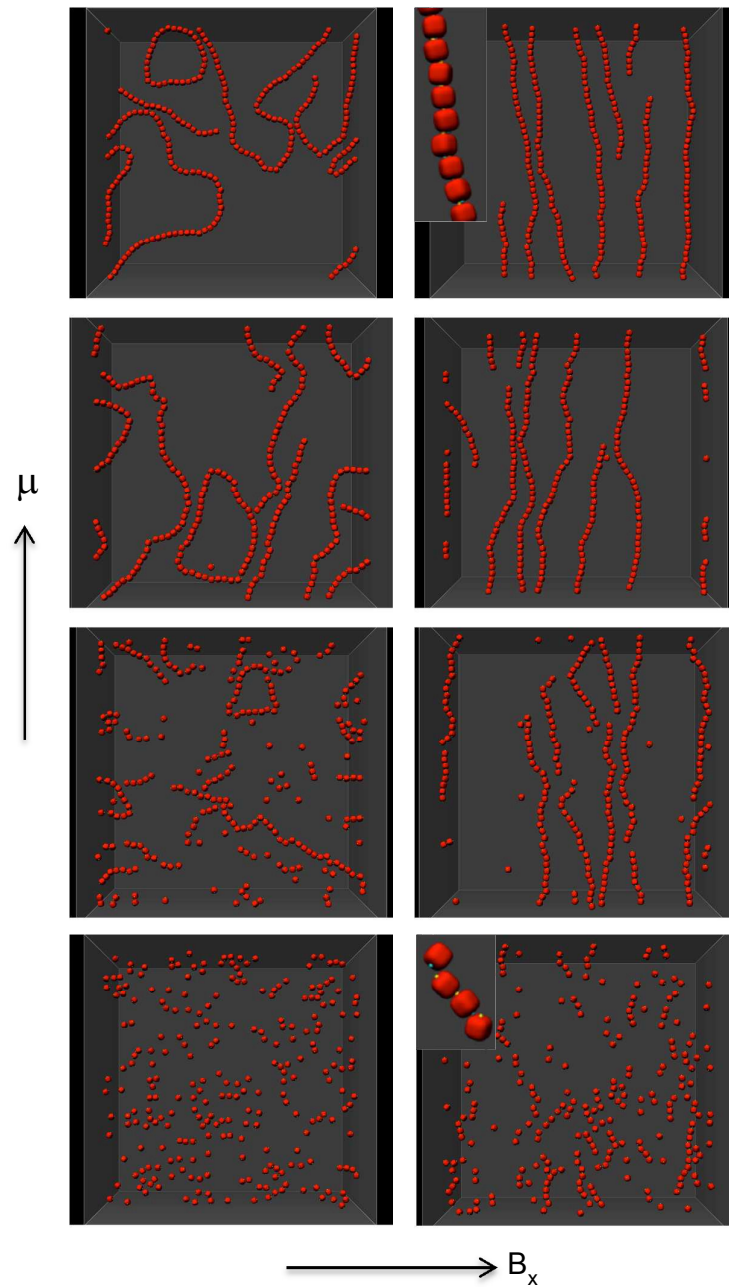


Fig. 6 Snapshots of quasi-2d fluids of superballs with dipole moments $\mu^* = 1.86$ (bottom), 2.24, 2.61, 2.98 (top) for dipoles in the 001-direction in the absence $B_x^* = 0$ (left) and presence of an external field $B_x^* = 0.632$ (right) applied parallel to the plane of the superballs. The inserts are four-fold magnified.

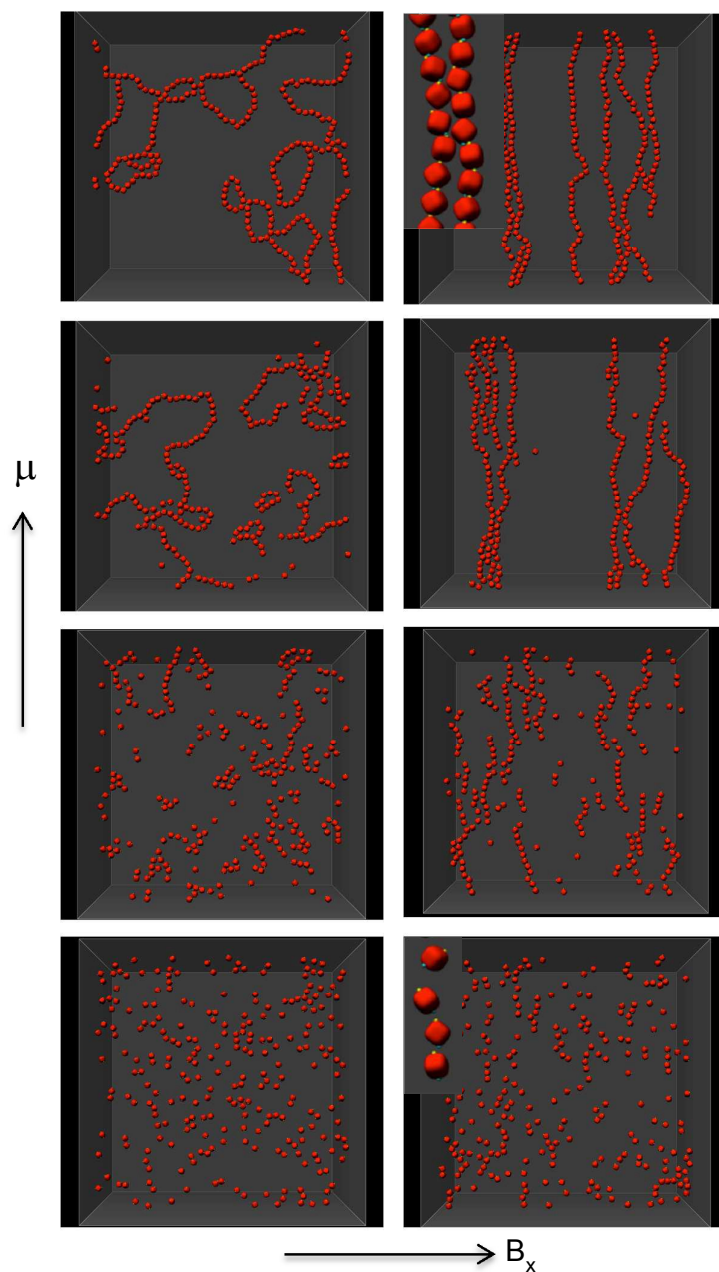


Fig. 7 Snapshots of quasi-2d fluids of superballs with dipole moments $\mu^* = 1.86$ (bottom), 2.24, 2.61, 2.98 (top) for dipoles in the 011-direction in the absence $B_x^* = 0$ (left) and presence of an external field $B_x^* = 0.632$ (right) applied parallel to the plane of the superballs. The inserts are four-fold magnified.

March 30, 15

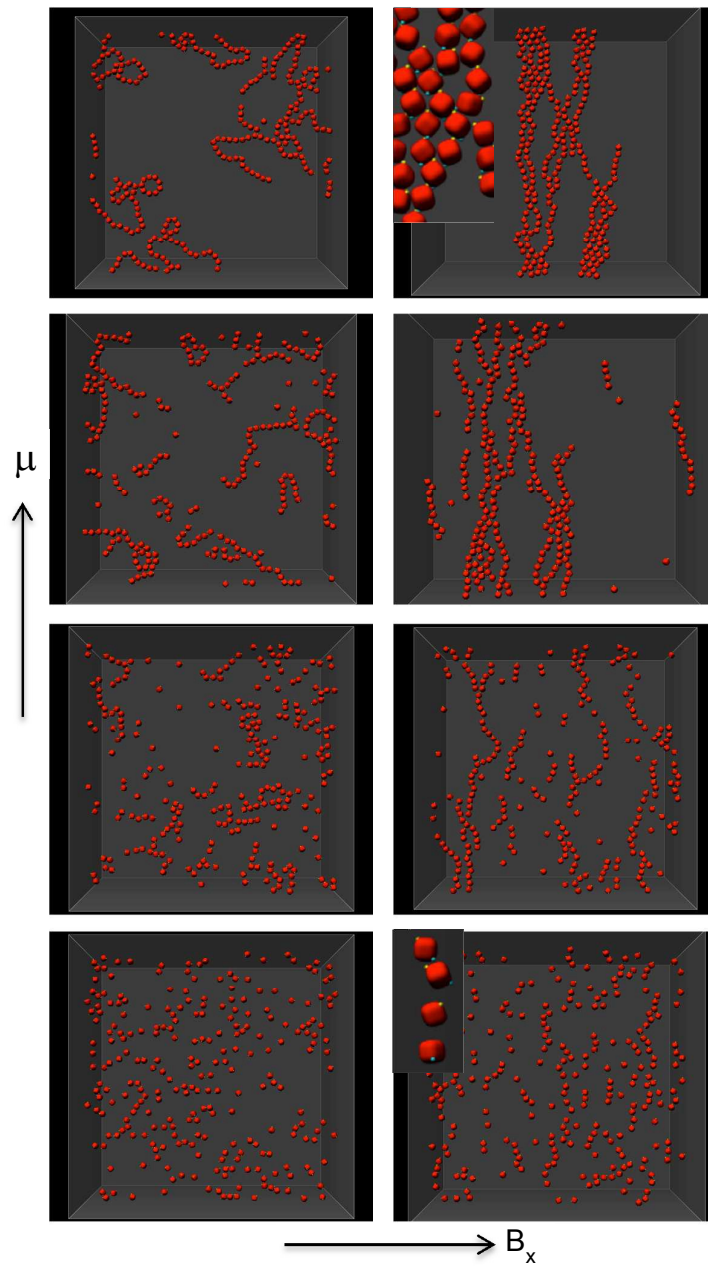


Fig. 8 Snapshots of quasi-2d fluids of superballs with dipole moments $\mu^* = 1.86$ (bottom), 2.24, 2.61, 2.98 (top) for dipoles in the 111-direction in the absence $B_x^* = 0$ (left) and presence of an external field $B_x^* = 0.632$ (right) applied parallel to the plane of the superballs. The inserts are four-fold magnified.

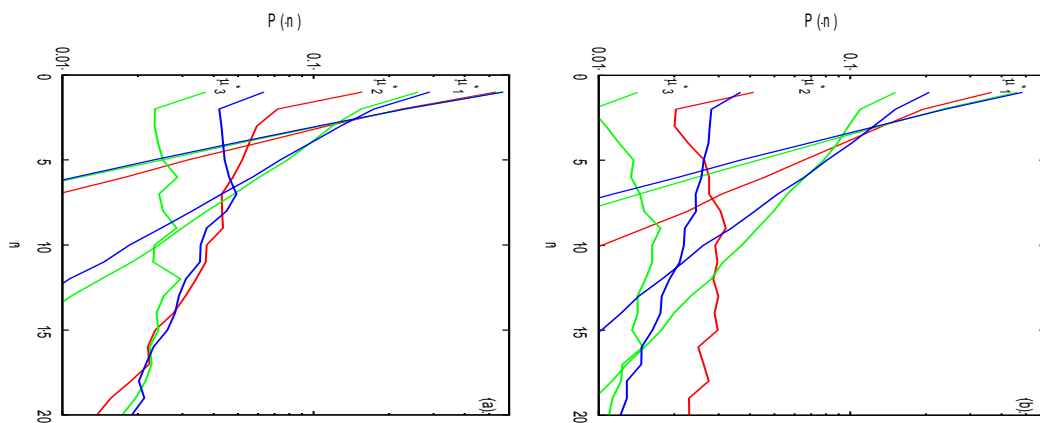


Fig. 9 Cluster size probability function $P(n)$ for dipoles in the (a) 001-direction (red), 011-direction (green), and 111-direction (blue) at indicated values of the dipole moment $\mu_1^* = 1.86$, $\mu_2^* = 2.24$, and $\mu_3^* = 2.61$, in the (a) absence and (b) presence of an external field $B_x^* = 0.632$. Data for the 001-direction at $\mu^* = \mu_3^*$ are outside the range selected.

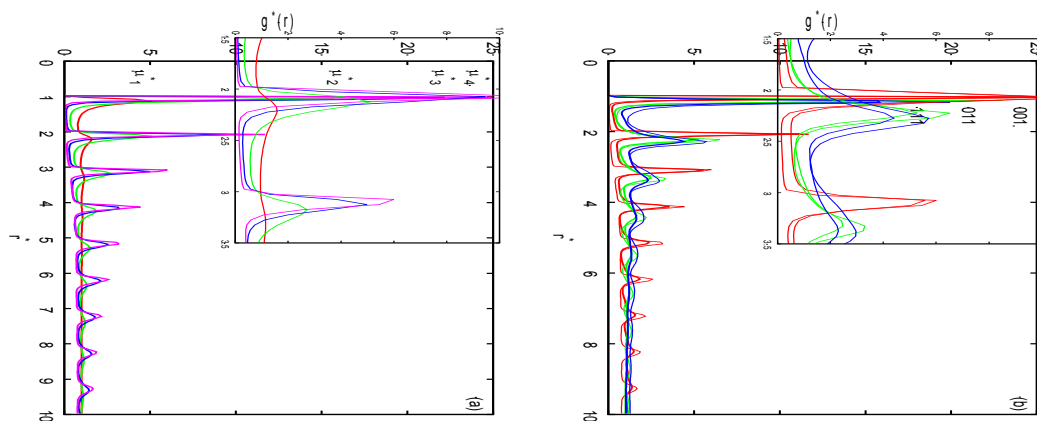


Fig. 10 Two-dimensional radial distribution function $g(r)$ for (a) dipole moments $\mu_1^* = 1.86$ (red), $\mu_2^* = 2.24$ (green), $\mu_3^* = 2.61$ (blue), and $\mu_4^* = 2.98$ (purple) with dipoles in the 001-direction in the absence of an external field and (b) dipole moment $\mu_4^* = 2.98$ for dipoles in the 001-direction (red), the 011-direction (green), and the 111-direction (blue) at the absence (thick curves) and presence (thin curves) of an external field with $B_x^* = 0.632$. Inserts display magnification of the second and third peaks.

March 30, 15

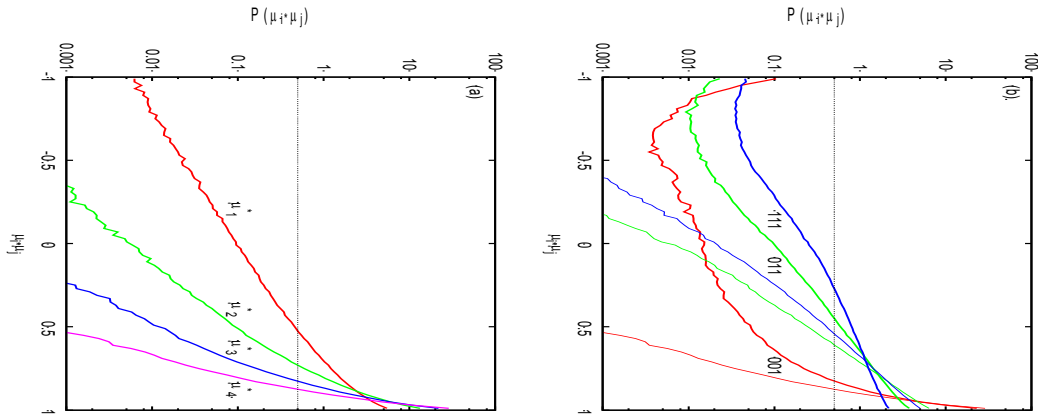


Fig. 11 Dipole–dipole angular probability function $P(\hat{\mu}_i \cdot \hat{\mu}_j)$ of neighboring superballs for (a) dipole moments $\mu_1^* = 1.86$ (red), $\mu_2^* = 2.24$ (green), $\mu_3^* = 2.61$ (blue), and $\mu_4^* = 2.98$ (purple) with dipoles in the 001-direction in the absence of an external field and (b) dipole moment $\mu_4^* = 2.98$ for dipoles in the 001-direction (red), the 011-direction (green), and the 111-direction (blue) in the absence (thin curves) and presence (thick curves) presence of an external field $B_x^* = 0.632$. Dashed lines represent a uniform probability distribution.

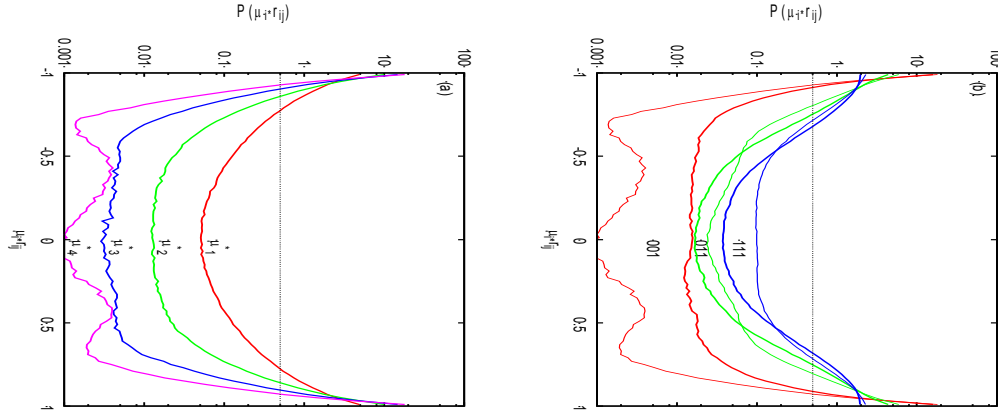


Fig. 12 Dipole–com-com-vector angular probability function $P(\hat{\mu}_i \cdot \hat{r}_{ij})$ of neighboring superballs for (a) dipole moments $\mu_1^* = 1.86$ (red), $\mu_2^* = 2.24$ (green), $\mu_3^* = 2.61$ (blue), and $\mu_4^* = 2.98$ (purple) with dipoles in the 001-direction in the absence of an external field and (b) dipole moment $\mu_4^* = 2.98$ for dipoles in the 001-direction (red), the 011-direction (green), and the 111-direction (blue) in the absence (thin curves) and presence (thick curves) of an external field $B_x^* = 0.632$. Dashed lines represent a uniform probability distribution.

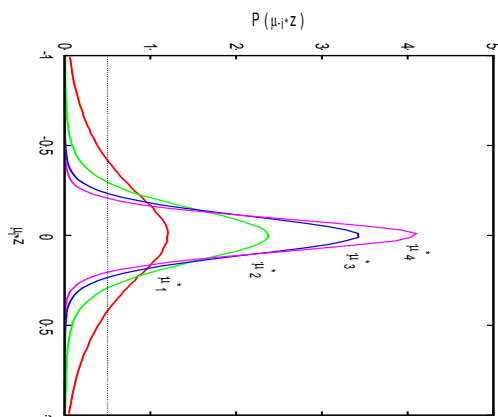
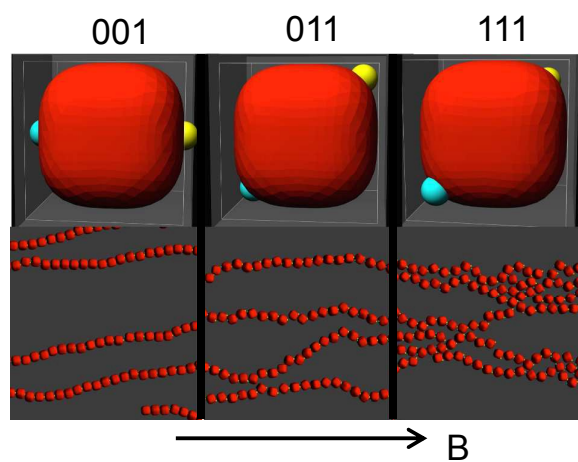


Fig. 13 Dipole–external-field angular probability function $P(\hat{\mu}_i \cdot \hat{\mathbf{z}})$ for dipole moments $\mu_1^* = 1.86$ (red), $\mu_2^* = 2.24$ (green), $\mu_3^* = 2.61$ (blue), and $\mu_4^* = 2.98$ (purple) with dipoles in the 001-direction in the presence of an external field $B_x^* = 0.632$. Dashed line represents a uniform probability distribution.

March 30, 15

TOC



Structures formed by dipolar superballs in an in-plane external field B depends on the direction of the dipole – chains are formed for a 001-direction and bundles for a 111-direction.